THE JOURNAL OF BIOLOGICAL CHEMISTRY VOL. 286, NO. 17, pp. 15308–15316, April 29, 2011

Identification of a Tetrameric Assembly Domain in the C Terminus of Heat-activated TRPV1 Channels*

Received for publication, January 25, 2011 Published, JBC Papers in Press, February 25, 2011, DOI 10.1074/jbc.M111.223941

Feng Zhang[‡], Shuang Liu[‡], Fan Yang[§], Jie Zheng[§1], and KeWei Wang[‡¶2]

From the [‡]Department of Neurobiology, Neuroscience Research Institute, Peking University Health Science Center, and [¶]Department of Molecular and Cellular Pharmacology, Peking University School of Pharmaceutical Sciences, 38 Xueyuan Road, Beijing 100191, China and the [§]Department of Physiology and Membrane Biology, University of California, Davis, California 95616

Transient receptor potential (TRP) channels as cellular sensors are thought to function as tetramers. Yet, the molecular determinants governing channel multimerization remain largely elusive. Here we report the identification of a segment comprising 21 amino acids (residues 752–772 of mouse TRPV1) after the known TRP-like domain in the channel C terminus that functions as a tetrameric assembly domain (TAD). Purified recombinant C-terminal proteins of TRPV1–4, but not the N terminus, mediated the protein-protein interaction in an *in vitro* pulldown assay. Western blot analysis combined with electrophysiology and calcium imaging demonstrated that TAD exerted a robust dominant-negative effect on wild-type TRPV1. When fused with the membrane-tethered peptide Gap43, the TAD blocked the formation of stable homomultimers. Calcium imaging and current recordings showed that deletion of the TAD in a poreless TRPV1 mutant subunit suppressed its dominant-negative phenotype, confirming the involvement of the TAD in assembly of functional channels. Our findings suggest that the C-terminal TAD in TRPV1 channels functions as a domain that is conserved among TRPV1–4 and mediates a direct subunit-subunit interaction for tetrameric assembly.

Transient receptor potential (TRP)[3] channels function as cellular sensors for numerous stimuli (1–3), and belong to a superfamily of cation channels with diverse functions (4). All TRP channels are thought to be tetramers assembled with 4-fold symmetry with a central ion permeation pore (4, 5). Each subunit of the TRP family contains six transmembrane segments (S1–S6) with a pore region between S5 and S6, and intracellular N- and C-terminal domains (5, 6). Members of the TRPV subfamily feature unique structural elements of the N-terminal ankyrin repeat domain (ARD) and C-terminal TRP domain immediately after the S6 transmembrane domain (5, 7, 8). The six members of the TRPV subfamily can be further divided into two groups: the nonselective and heat-activated TRPV1–4 primarily expressed in sensory neurons and keratinocytes, and highly Ca^{2+} selective TRPV5–6 channels primarily expressed in epithelial tissues (6, 9, 10). Heat-activated TRPV1–4 channels are activated by temperature, voltage, protons, and chemicals, and are responsible for maintenance of homeostasis and sensation of environmental changes (11–14). Therefore, understanding the rules governing subunit assembly of heat-activated TRPV1–4 channels has important implications for channel physiology and pharmacology.

Biochemical and functional studies suggest that TRP channels form homomeric or heteromeric complexes depending on subunit types (15–18). One potential domain determining subunit assembly is the ARD. The structure of TRPV channels features six ARD in the N-terminal cytosolic domain (19). Each ARD is a short sequence, typically 33 amino acids, forming an anti-parallel helix-turn-helix structure followed by a β– hairpin loop (19, 20). Ankyrin repeats generally serve as a protein-protein interaction motif (21, 22), and the ARD of TRPV6 is considered to be essential for channel assembly (19, 23). However, size exclusion chromatography and crystal packing analysis of TRPV subunits reveal that ARD does not assemble as a tetramer and is monomeric in solution even at high concentrations (19, 23), indicating that the N-terminal ARD is unlikely to mediate tetramerization of functional TRPV channels.

The intracellular C-terminal region has also been proposed to contribute to subunit assembly. Besides harboring phosphoinositide and calmodulin binding domains, and protein kinase C (PKC) consensus sites (24–26), the cytosolic C terminus of TRPV has a TRP-like domain containing a TRP box that is a conserved signature sequence following the last transmembrane segment (5). Biochemical and functional studies have attributed to the TRPV C terminus an important role in channel subunit multimerization (17, 27, 28). García-Sanz *et al.* (17) proposed that the TRP-like domain in TRPV1 is a molecular determinant of subunit tetramerization into functional channels. Yet, based on a proposed molecular model in which the TRP-like box of TRPV1 adopts an anti-parallel β-strand conformation (27), this structural arrangement of the TRP-like box appears to fold into an α-helix secondary structure that is unlikely to mediate the protein-protein interaction (27). Therefore, the role of the TRP-like box of the C terminus in channel assembly has been unclear and remains controversial.

Despite extensive studies, mechanisms that direct heat-activated TRPV channel assembly and the specificity of subunit interactions still remain largely elusive. In this study, we investigated the homomultimerization of heat-activated TRPV1

* This work was supported by National Science Foundation of China Research Grants 30630017 and 30970919 (to K. W. W.), Ministry of Science Technology of China "973 Program" 2007CB512100, and Ministry of Education of China 111 Project China B07001.

[1] To whom correspondence may be addressed. Tel.: 530-7521241; E-mail: jzheng@ucdavis.edu.

[2] To whom correspondence may be addressed. Tel.: 8610-82805065; E-mail: wangkw@bjmu.edu.cn.

[3] The abbreviations used are: TRP, transient receptor potential; TAD, tetrameric assembly domain; ARD, ankyrin repeat domain; MBP, maltose-binding protein.

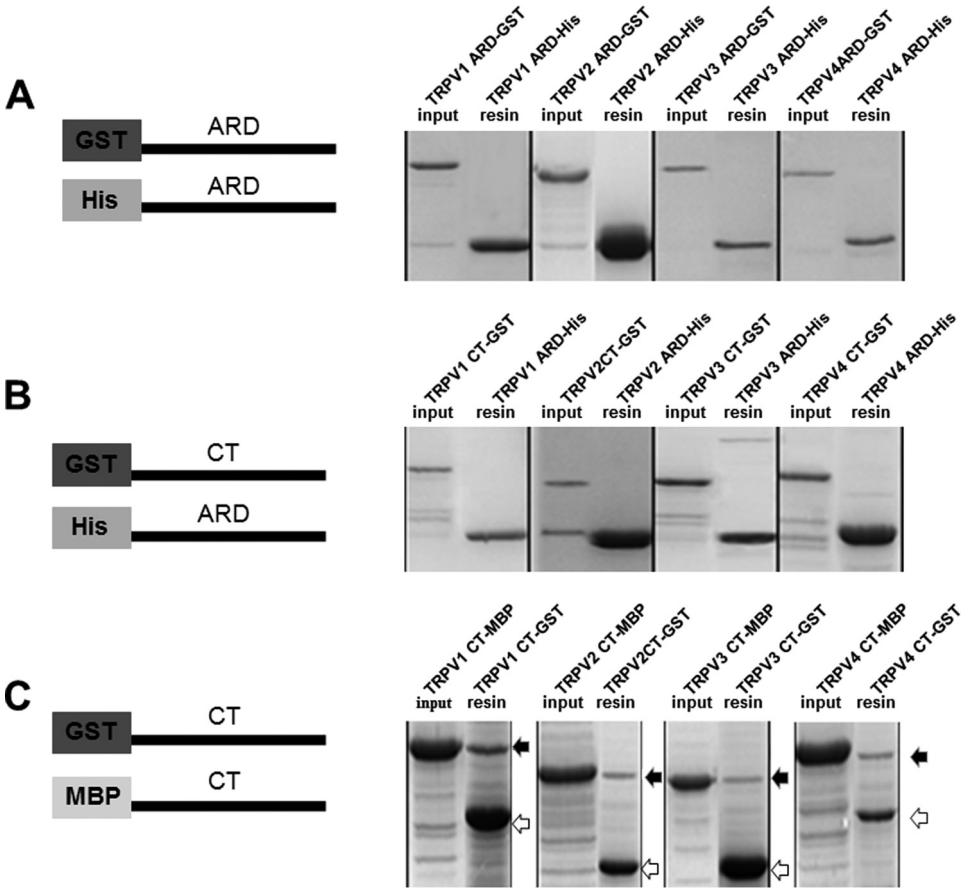

FIGURE 1. **Homomeric association mediated by the C terminus of heat-activated TRPV1–4 *in vitro*.** *A*, *left panel*, schematic illustrating the N-terminal ARD with GST or His_6 fusion tags used for protein purification and pulldown analysis. *Right panel* shows the pulldown assay carried out between each N-ARD of TRPV1–4. *B*, *left panel*, schematic illustrating the N-terminal ARD with the His_6 tag and C-terminal constructs with the GST tag; *right panel* shows the pulldown assay carried out between each N-ARD and C terminus of TRPV1–4. *C*, *left panel*, schematic illustrating the constructs of TRPV1–4 C termini subunits fused with GST or MBP tags for evaluation of protein-protein interaction. *Right panels*, *filled* and *open arrows* represent the input of fusion proteins (TRPV1–4 C terminus with MBP tag) and resin ingredients (TRPV1–4 C terminus with GST tag), respectively.

channels. By analysis of Western blotting and pull down between cytosolic N and C termini of TRPV channels, we identified a segment following the known TRP domain (coiled-coil domain) in the channel C terminus that functions as a TAD. Calcium imaging and electrophysiology further confirm that the TAD mediates the functional assembly of heat-activated TRPV1 channels.

MATERIALS AND METHODS

Molecular Biology—Mouse TRPV1–TRPV4 C terminus cDNAs were subcloned between BamHI and XhoI sites of vector pGEX-6P1 and modified pMAL-C2 for prokaryotic expression, respectively. The ARD from the N terminus of mTRPV1–4 were subcloned into NdeI and XhoI sites of the pEt21b vector or BamHI and XhoI sites of the pGEX-6P1 vector. The deletion mutations and poreless TRPV1 mutant (Δ628–646, plTRPV1) were generated by overlapping PCR. The cytoplasmic protein Gap43 (growth associated protein 43) comprising the N-terminal 20 amino acids, the sequence of which targets Gap43 to lipid rafts via a dual palmitoylation (29), was generated by primers CTAGCTAGCATGCTGTGCTGTATGAG (forward) and GTCAAGCTTGATCTTTTGGTCCTCA (reverse) using plasmid EGFP-mem (Clontech) as template. All restriction enzymes were purchased either from New England Biolabs, Inc. or Takara. All cDNA fragments were amplified using LA Taq (TAKARA, Dalian), and inserts of all clones were confirmed by sequencing.

Biochemistry and Pulldown Assay—For protein production, purification, and *in vitro* interaction assays, all cDNA constructs in either pGEX-6P1 and modified pMAL-C2 vectors were transfected and expressed in *Escherichia coli* BL21 (Rosetta). Rosetta cells were cultured in LB at 37 °C and induced at A_{600} = 0.5 with 50 mM isopropyl 1-thio-β-D-galactopyranoside at 22 °C for 8–16 h. The cells were harvested by centrifugation at 5000 × *g* for 15 min at 4 °C, and resuspended in buffer (25 mM Tris, pH 8.0, 150 mM NaCl) supplemented with protease inhibitors. The cells were lysed by sonication, and the insoluble fragments were removed by centrifugation at 14,000 × *g* for 1 h. The supernatants were loaded into previously equilibrated 1-ml GST4B resin (GE Healthcare), amylose resin (New England Biolabs), and HiTrap Ni^{2+} chelating columns (Amersham Biosciences) at a rate of 1 ml/min, respectively. After washing the columns, the bound epitope proteins, such as GST (glutathione *S*-transferase)-, His_6 (hexa-histidine)-, and MBP (maltose-binding protein)-tagged N or C terminus TRPV1–4, were eluted and stored at −80 °C for pulldown assays. To test interactions between TRPV1–4 N-terminal ARD and the C

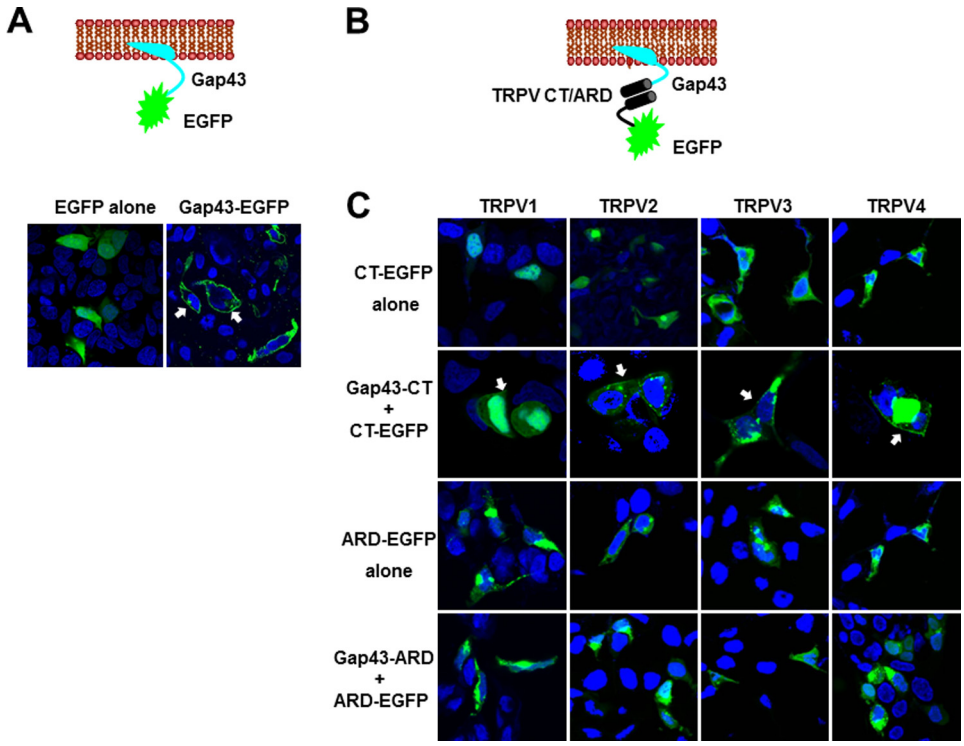

FIGURE 2. **Interactions mediated by the C terminus of TRPV1–4 in confocal imaging of HEK293T cells.** *A*, *top panel*, schematic illustrating the EGFP-tagged peptide Gap43 tethered to the cell membrane, and the *bottom panel* shows the confocal images of fluorescence in HEK293T cells transfected with EGFP alone as a control and Gap43-EGFP proteins (*filled white arrows* for membrane fluorescence). *B*, schematic illustrating detection for the C terminus or ARD tagged with EGFP, and interaction between Gap43-fused C terminus or ARD of TRPV1–4. *C*, confocal images showing the fluorescence of the C terminus-tagged with EGFP (*first panel*), and membrane-tethered TRPV1–4 C terminus that is capable of redistribution of corresponding EGFP-tagged C terminus (the *second panel* and *filled white arrows*), but Gap43-tagged ARD could not change the distribution patterns of the corresponding EGFP-tagged ARD (the *third* and *fourth panels*).

terminus, ~100 μg of GST- and His_6-tagged proteins were bound to nickel and GST4B resins, respectively. For flow-through of the nickel or GST4B resins, ~200 μg of MBP-tagged and GST-tagged TRPV1–4 C terminus or GST-tagged ARD were loaded onto the column. After an extensive wash of the column, ~10 μl of resin was loaded on SDS-PAGE gels and visualized by Coomassie Brilliant Blue R-250.

Western Blotting—24 h after transfection HEK293T cells were lysed in 100 μl of ice-cold lysis buffer RIPA (50 mM Tris-HCl, 150 mM NaCl, 1% Nonidet P-40, pH 7.4) with protease inhibitor mixture (1 times) for 30 min on ice. Cell lysates were then centrifuged at 4 °C for 10 min at 14,000 × *g*. Supernatants were denaturated with SDS-PAGE sample buffer containing 1 M DTT (95 °C, 5 min), separated by 12% SDS-PAGE, and probed by Western immunoblotting using anti-FLAG (1:4000, Sigma) overnight at 4 °C. For controls, β-actin was blotted with an anti-actin antibody at 1:5,000 dilution (Zhongshan Goldenbridge Biotech, Beijing), and immunoreactive bands were visualized with Western lightning chemiluminescence reagents (Millipore).

Confocal and Calcium Imaging—HEK293T cells were maintained at 37 °C under 5% CO_2 in DMEM supplemented with 10% fetal bovine serum. For confocal imaging and calcium imaging experiments, cells were reseeded on glass or chambered coverglass coated with poly-D-lysine for detection. All the constructs were transfected using Lipofectamine 2000 (Invitrogen) following the manufacturer's instructions. For confocal imaging, 1 day after transfection, HEK293T cells were washed with phosphate-buffered saline (PBS, pH 7.4) three times before fixing with 4% paraformaldehyde in PBS for 10 min. Nuclei were stained using Hoechst 33258 (Molecular Probes). Images were acquired using a Leica laser-scanning confocal system (TCS SP5II).

For calcium imaging, HEK293T cells were cotransfected with rTRPM8, mTRPV1, and Gap43-tagged C terminus (Gap43-CT), N terminus (Gap43-NT), or TAD at different molar ratios. Two days after transfection, cells were loaded with 5 μM Fluo-3AM (Biotium, Hayward, CA) in 0.02% F-127, and incubated in 2 mM Ca^{2+} Ringer's solution (140 mM NaCl, 5 mM KCl, 2 mM $MgCl_2$, 10 mM glucose, 2 mM $CaCl_2$, 10 mM HEPES, pH 7.4) at 37 °C for 30–60 min. After loading, cells were then washed with Ringer's solution and equilibrated in 200 μl of Ringer's solution. For activation of TRPV1 and TRPM8 channels in HEK293T cells, 200 μl of 300 nM TRPV1, a specific agonist capsaicin (150 nM final), and 1.5 mM TRPM8, a specific agonist menthol (0.5 mM final), were added at the indicated time points. Data were normalized and averaged from all menthol-sensitive cells in the field.

Two-electrode Voltage Clamp Recording—All cRNAs were *in vitro* transcribed from linearized plasmids (in KSM vectors) using the T3 mMESSAGE mMACHINE Kit (Ambion). *Xenopus* oocytes (stage V–VI) were selected and defoliculated by treatment with collagenase (30), and then were injected with 46 nl of solution containing 0.5–4.0 ng of cRNA from mouse TRPV1 or rat TRPM8 using a microinjector (Drummond Scientific Co). Oocytes were then kept at 17 °C in ND96 solution

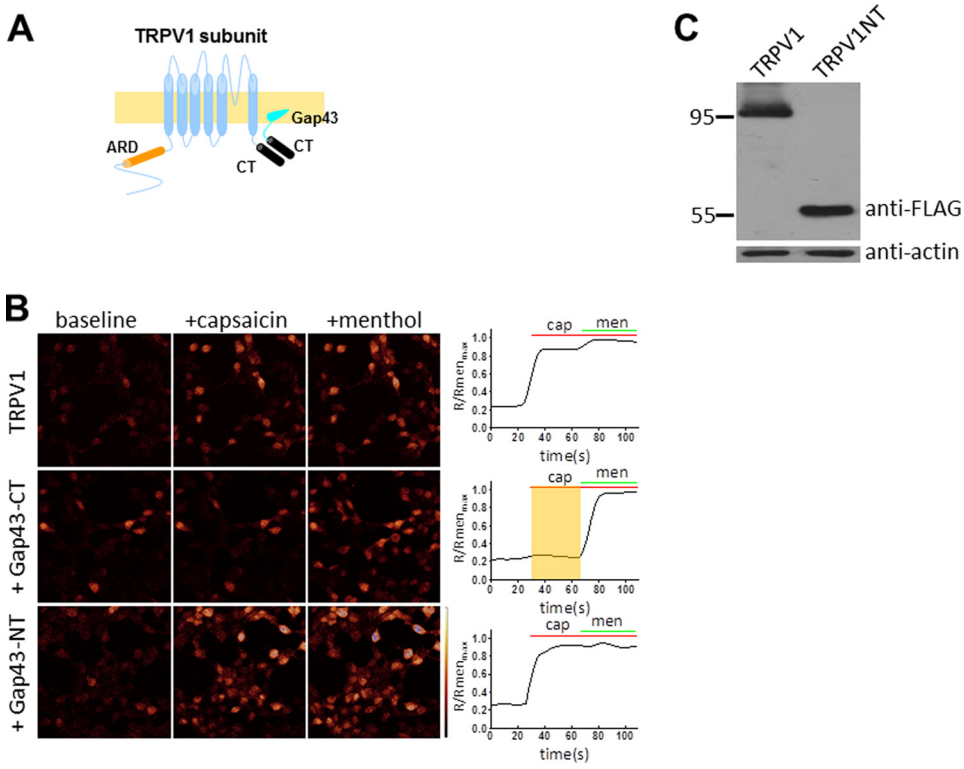

FIGURE 3. **Inhibition of TRPV1 channel function by its C terminus in calcium imaging of HEK293T cells.** *A*, schematic illustrating the TRPV1 subunit interaction between the membrane-tethered C terminus (*Gap43-CT*). TRPV1 C terminus (*black cylinders*) is fused to the membrane-tethered Gap43 (*light cyan*). *B*, confocal images of HEK293 cells that were TRPV1 and TRPM8 co-transfected with or without Gap43-CT (TRPV1 C terminus) or Gap43-NT (TRPV1 N terminus) and subjected to channel activation by 150 nM capsaicin and 500 μM menthol. *Top panel*, co-transfection of TRPV1 and TRPM8 at a mole ratio of 1:1; *middle panel*, co-transfection of TRPV1 and TRPM8 with Gap43-CT at the ratio of 1:1:5; *bottom panel*, co-transfection of TRPV1 and TRPM8 with Gap43-NT at the same ratio (1:1:5). *Right panel*, semi-quantitative measurements of fluo-3AM from results of the corresponding *left panel*; each trace is an average of 27–43 cells. Applications of capsaicin (*cap*, 150 nM) and menthol (*men*, 500 μM) are indicated as *green* and *red lines*, respectively. The *shaded* area in the *middle panel* indicates the lack of response to capsaicin. *C*, Western blotting of the cell lysate of HEK29T transfected with FLAG-tagged TRPV1 and Gap43-CT (*middle panel* in *B*) or TRPV1 and FLAG-tagged Gap43-NT (*bottom panel* in *B*), Western blot results are blotted with anti-FLAG or anti-actin, respectively. Molecular mass standards are indicated as kDa.

(96 mM NaCl, 2 mM KCl, 1.8 mM $CaCl_2$, 1 mM $MgCl_2$, 10 mM HEPES, pH 7.4). 48 h after injection, whole cell current recordings by two-electrode voltage clamp were performed at room temperature in Ca^{2+}-free ND96 solution (supplemented with 0.1 mM $BaCl_2$) with a GeneClamp500 amplifier (Axon Instruments). Data were acquired using Patchmaster software (HEKA) and digitized at 1.0 kHz using an ITC-16 (Instrutech Corp.). Electrodes were filled with 3 M KCl with resistances of 0.5–1.0 megaohm.

RESULTS

C Terminus of Heat-activated TRPV1–4 Mediates Homomeric Interactions—To delineate the role of the cytoplasmic N-terminal ankyrin repeat domain (N-ARD) or C terminus in mediating homomeric interactions of TRPV1–4 subunits, we started by generating N-ARD or C-terminal constructs tagged with GST, His_6, or MBP epitopes for protein expression and purification (Fig. 1, *A–C*, *left panels*). The evaluation of protein-protein interactions between tagged proteins was analyzed by *in vitro* pulldown assay. Fig. 1*A* (*right panel*) shows that there were no interactions between the His_6-tagged N-terminal ARD (N-ARD) of TRPV1–4 and GST-tagged N-ARD. Similarly, the His_6-tagged N-ARD and GST-tagged C terminus also had no interactions (Fig. 1*B*, *right panel*). In contrast, the GST-tagged C terminus and MBP-tagged C-terminal proteins of TRPV1–4 subunits showed a robust interaction by forming their individual complexes (Fig. 1*C*, *right panel*), suggesting that the C termini are capable of associating with each other and mediating the subunit-subunit interaction.

To evaluate the interaction between N-ARD or the C terminus of TRPV1–4 in HEK293T cells, we generated TRPV1–4 N-ARD or C terminus fusion proteins fused to the membrane-tethered peptide Gap43. Gap43 is 20 amino acids long, containing a signal for post-translational palmitoylation of cysteines that targets the membrane (29). As a positive control, the membrane-tethered peptide Gap43 is tagged with EGFP for visualization of membrane fluorescence in confocal imaging (Fig. 2*A*). Expression of Gap43-tagged EGFP shows the membrane-localized fluorescence in HEK293T cells, compared with the dispersed expression pattern of EGFP alone proteins (Fig. 2*A*), suggesting that Gap43 is successfully tethered to the membrane. We reasoned that if there is an interaction between the N-terminal ARD and/or C terminus, we would be able to detect membrane fluorescence as a result of interaction between Gap43-CT (C terminus) and its associated proteins when co-expressed (Fig. 2*B*). As a negative control, the TRPV1–4 C terminus-tagged EGFP (CT-EGFP) alone shows a nuclear and diffused distribution of expression (Fig. 2*C*, *top panel*). When co-expressed with CT-EGFP (C terminus-tagged EGFP), the

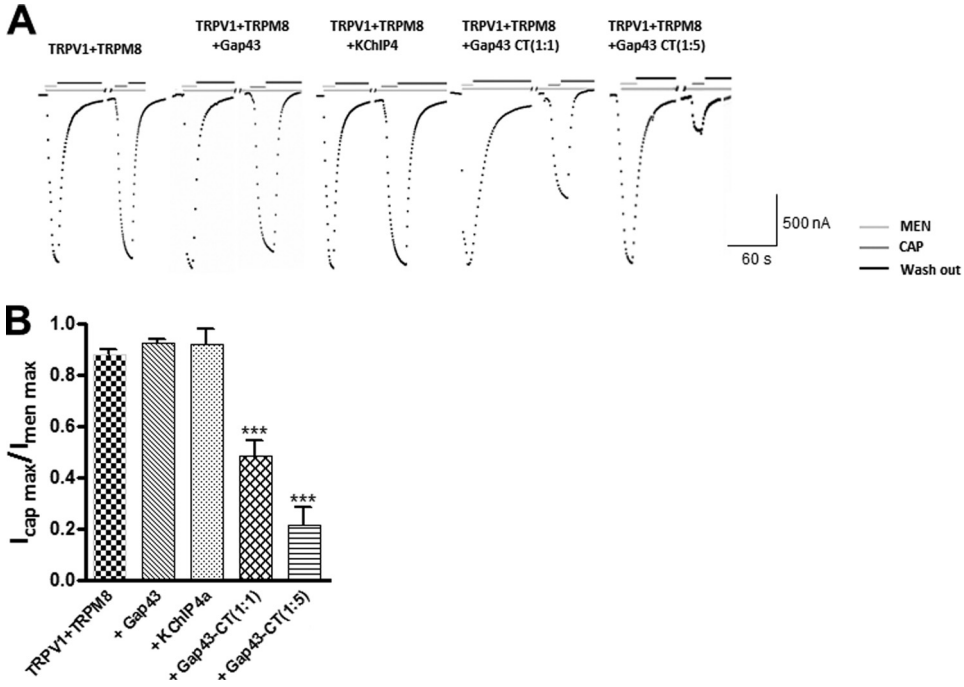

FIGURE 4. **Inhibition of TRPV1 channel function by membrane-tethered C terminus in *Xenopus* oocytes.** *A*, dominant-negative effect of the membrane-tethered C terminus on the TRPV1 channel function. In response to menthol and subsequent capsaicin, representative current traces were recorded from *Xenopus* oocytes expressing TRPM8 and TRPV1 (baseline) with Gap43 alone (blank control), KChIP4a (negative control), or membrane-tethered Gap43 C terminus at the ratios as indicated. Applications of menthol (500 μM final) and capsaicin (250 nM final) are shown in *green* and *red bars*, respectively. The *dashed line* indicates zero-current. *B*, current amplitude comparison of maximal capsaicin-induced currents normalized to maximal menthol-induced currents from *panel A*, showing the effect of the increasing ratio of Gap43-CT on TRPV1 (n = 5–9 cells). Statistical significance is indicated as *asterisks*, ***, $p < 0.001$.

membrane-tethered Gap43-CT (Gap43-tagged C terminus) was capable of redistributing the CT-EGFP proteins on the membrane (Fig. 2*C*, *second panel*), indicating that the C terminus of TRPV1 could interact with the membrane-tethered C terminus (Gap43-CT) to form a complex. However, co-expression of membrane-tethered Gap43-ARD (Gap43-tagged N-ARD) and ARD-EGFP (ARD-tagged EGFP) led to no redistribution of fluorescence (Fig. 2*C*, *bottom panel*), as compared with the ARD-EGFP alone (Fig. 2*C*, *third panel*), suggesting that N-ARD does not interact to form homomeric complexes. Together with the data from the pulldown assay, these results allowed our attention to focus on the C terminus of TRPV channels.

Inhibition of Functional Assembly of TRPV1 by Its Membrane-tethered C Terminus—To functionally confirm the role of the C terminus in homomeric assembly, we co-transfected HEK293T cells with Gap43-CT (TRPV1 C terminus fused to Gap43) and wild-type (WT) TRPV1 (Fig. 3*A*), and measured the fluorescence calcium signal in confocal imaging. As a positive control, TRPM8 was co-transfected to serve as an internal reference for transfection and channel expression. Compared with the baseline fluorescence, co-expression of TRPV1 and TRPM8 (at a mole ratio of 1:1) showed a robust calcium fluorescence signal in response to the TRPV1 agonist capsaicin (150 nM) with a noticeable subsequent activation by application of the TRPM8 agonist menthol (500 μM) (Fig. 3*B*, *top panels*), indicating that the calcium signal resulted from activation of TRPV1 and TRPM8 channels, respectively. In contrast, coexpression of TRPV1 and TRPM8 with membrane-tethered Gap43-CT (TRPV1 C terminus) at a 1:1:5 ratio (TRPV1:TRPM8:Gap43-CT) led to no activation of the capsaicin-induced calcium signal, whereas activation of TRPM8 function by menthol was observed (Fig. 3*B*, *middle panels*), indicating that Gap43-CT exerted a robust dominant-negative effect on WT TRPV1 channels. In contrast, coexpression of TRPV1 and TRPM8 with Gap43-NT (TRPV1 N terminus) at the same ratio (1:1:5 for TRPV1:TRPM8:Gap43-NT) had no inhibitory effect on the calcium signal induced by capsaicin (Fig. 3*B*, *bottom panels*), demonstrating that the N terminus of TRPV1 does not associate with WT TRPV1 to affect the channel function. To further confirm that the lack of a functional response to capsaicin was not due to the low expression level of TRPV1, we used Western blots to detect TRPV1 expression. Fig. 3*C* shows that both TRPV1 and the N terminus of TRPV1 were robustly expressed, further confirming that the inhibitory effect on WT TRPV1 resulted from coexpression of Gap43-CT. These results indicate that the C terminus of TRPV1 channels mediates the homomeric assembly.

Dominant-Negative Phenotype of Membrane-tethered C Terminus on Function of TRPV1 Channels Expressed in Xenopus Oocytes—To further confirm the inhibitory effect of the C terminus on TRPV1 function, we co-expressed the membrane-tethered Gap43-CT (C terminus of TRPV1) with WT TRPV1 in *Xenopus* oocytes and recorded the current amplitude activated by capsaicin and menthol. Coexpression of TRPV1 and TRPM8 at a 1:1 ratio evoked similar current amplitudes first activated by menthol (500 μM) and followed by capsaicin (250 nM) (Fig. 4*A*). As controls, coexpression of TRPV1 and TRPM8 with Gap43 or KChIP4a (at mole ratio of 1:1:1) gave rise to similar current amplitudes activated by menthol (500 μM) and subsequently capsaicin (250 nM) (Fig. 4, *A* and *B*). In contrast, for

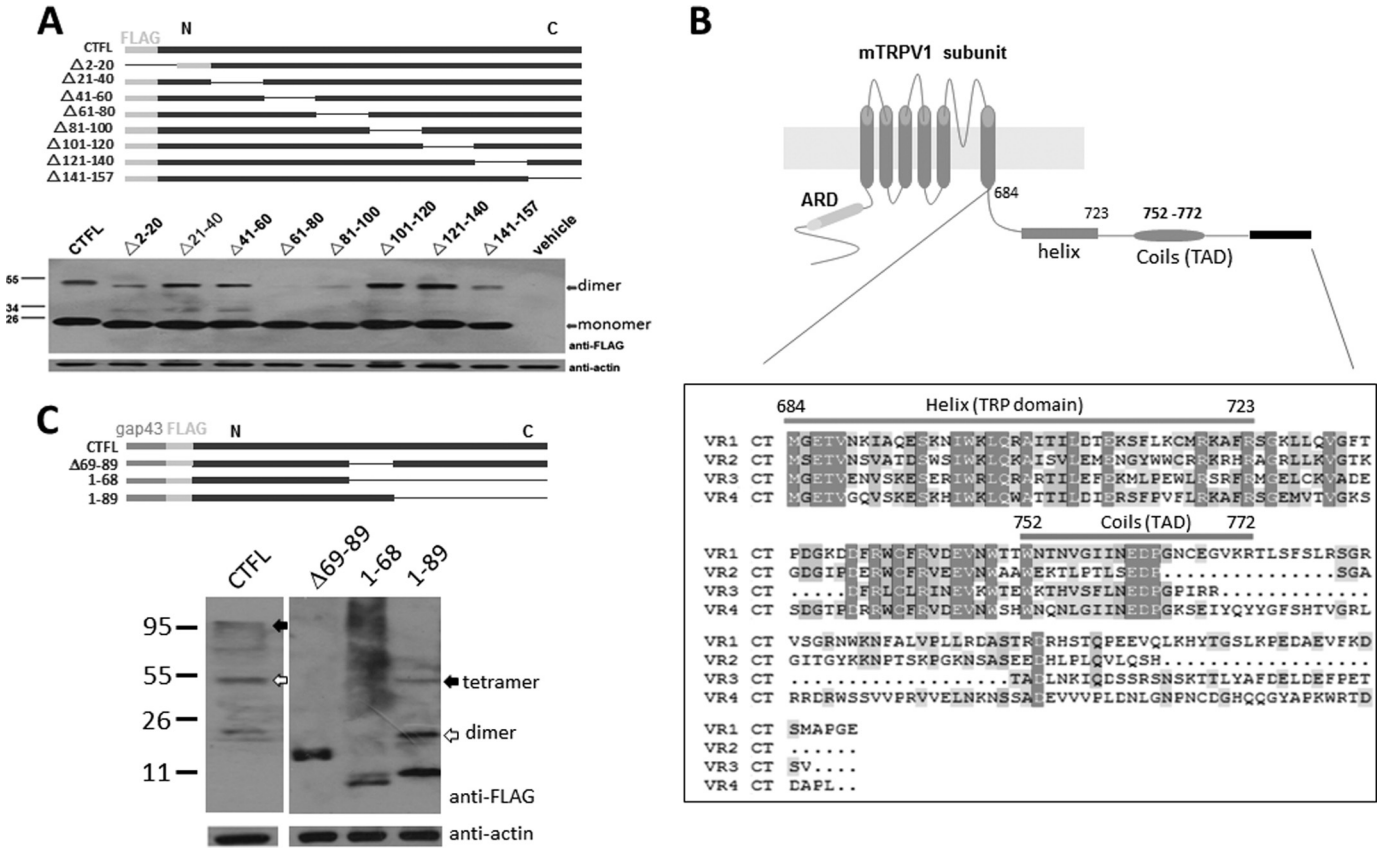

FIGURE 5. **Identification of C-terminal residues 69–89 as a TAD in TRPV1 subunit.** *A, top panel*, schematic representing TRPV1 C-terminal mutations generated for analysis of dimer formation, in which the *thin blue lines* indicate the deleted regions and *solid blue boxes* represent the cytoplasmic C-terminal coding regions. The *solid green boxes* indicate the FLAG tag fused to the N-terminal proteins for Western blot analysis. In the *bottom panel*, Western blot analysis shows dimer formation (*filled arrow*) between the full-length C terminus (*CTFL*) and its truncated forms as indicated. *B*, schematic diagram indicating the secondary structure prediction of the TRPV1 C terminus and sequence alignment of the heat-activated TRPV1–4 C termini, illustrating the TRP domain and the TAD identified. *C*, *top panel*, schematic representing deletions of the C terminus, in which *thin blue lines* indicate the deleted regions and *solid blue boxes* represent the cytoplasmic C-terminal coding regions. The *solid green* and *red boxes* indicate the FLAG tag and Gap43 fused to the proteins for Western blot analysis. In the *bottom panel*, Western blot analysis shows formation of the dimer (*open arrows*) and tetramer (*solid arrows*) between the full-length C terminus and its truncated forms as indicated. Molecular mass standards are indicated as kDa.

coexpression of TRPV1 and TRPM8 with a Gap43-CT ratio of 1:1:1, the capsaicin-activated TRPV1 current was reduced by about 40% with the normalized current changed from 0.88 ± 0.02 to 0.48 ± 0.05 ($n = 5–9$) (Fig. 4, *A* and *B*). By increasing the amount of Gap43-CT to a ratio of 1:1:5 (TRPV1:TRPM8: Gap43-CT), the inhibition of the capsaicin-induced current by Gap43-CT was increased to about 77% ($n = 5–8$) (Fig. 4). These results show that Gap43-CT (C terminus of TRPV1) can exert a dominant-negative effect on TRPV1 function by directly associating with the channel C terminus, further confirming the role of the C terminus in homomeric assembly of functional TRPV1 channels.

Identification and Functional Confirmation of a TAD for Homomeric Interactions—To identify residues critical in mediating the homomeric interaction within the C terminus, we then made a series of deletions within the C terminus by generating constructs tagged with a FLAG epitope (Fig. 5*A*, *top panels*). The homodimeric interactions between the deletion mutants within the C-terminal region were evaluated by Western blot analysis. As a control, the full-length C terminus of TRPV1 (157 amino acids) shows a clear dimer formation (Fig. 5*B*, *bottom panel*), which is consistent with our pulldown data and the literature report for TRPV1 C-terminal complexes that appear to be SDS-resistant (17). In contrast, deletion of residues 61–80 (residues 744–763 in full-length mTRPV1) and 81–100 (764–783 amino acids) resulted in an almost complete loss of dimer formation, compared with other deletion mutants that still retained the dimeric association (Fig. 5*A*, *bottom panel*), suggesting that residues 61–100 contain a critical domain in mediating protein-protein interaction. To further define residues in this domain involved in the interaction of C terminus, we used SwissProt modeling (EXPASY) to predict the TRPV1 C-terminal structure, which shows residues 69–89 (residues 752–772 of the full-length) are apt to adopt a secondary coil structure flanked by the β-strand structure (Fig. 5*B*). Based on the structure prediction, we generated constructs of deletion mutants (Δ69–89, 1–68, and 1–89) and fused both the Gap43 and FLAG tag to their N termini (Fig. 5*C*, *top panel*). The results show that the deletion mutant (Δ69–89) and residues 1–68 also disrupted the dimeric association, whereas mutant (1–89) remained in the dimeric and tetrameric assembly (Fig. 5*C*, *bottom panel*). This result confirms that C-terminal residues 69–89 likely serve as a TAD to mediate homomeric assembly of TRPV1 subunits.

To further confirm the role of residues 69–89 in tetrameric assembly, we co-expressed TRPV1 and Gap43-TAD, together

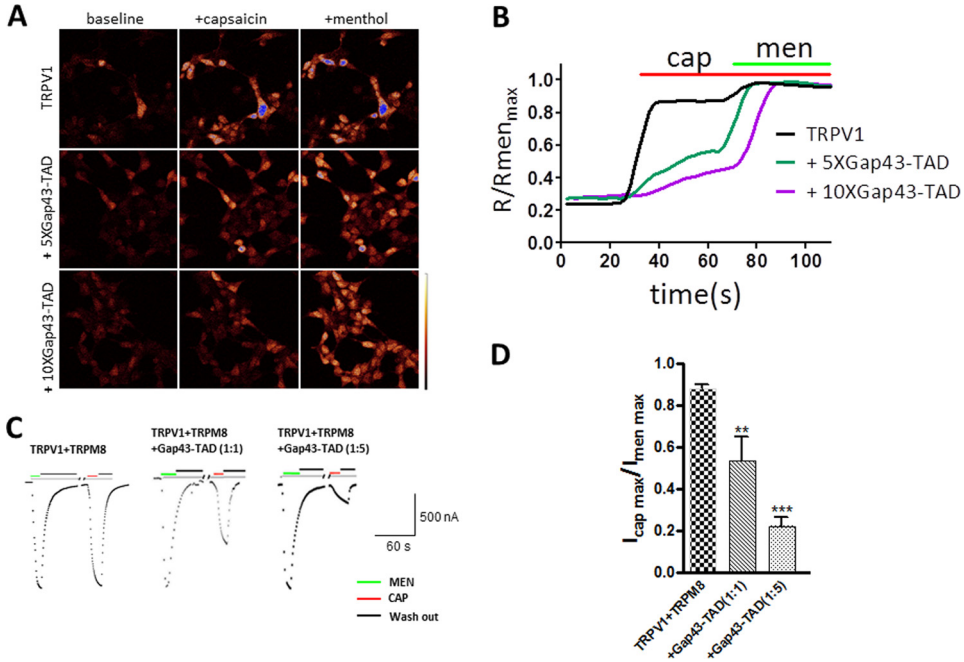

FIGURE 6. **Dominant-negative effect of membrane-tethered TAD on TRPV1 channel function.** *A*, calcium imaging of HEK293T cells co-transfected with TRPM8-, TRPV1-, and Gap43-tagged TAD with mole ratios of 1:1:5 or 1:1:10 (indicated as *5X* or *10X*), and then subjected to channel activation by 150 nM capsaicin and subsequent 500 μM menthol. *B*, normalized calcium imaging traces of TRPV1 (*black*) and TRPV1 + 5X (*green*) or 10X Gap43-TAD (*purple traces*) from the transfected HEK293T cells corresponding to *A*; each trace is an average of 19–43 cells. Applications of capsaicin (*cap*, 150 nM) and menthol (*men*, 500 μM) are indicated as *green* and *red lines*, respectively. *C*, representative current traces recorded from *Xenopus* oocytes coexpressing TRPM8 and TRPV1 with Gap43-TAD at mole ratios of 1:1:1 or 1:1:5. Applications of menthol (500 μM) and capsaicin (250 nM) are shown in *green* and *red bars*, respectively. *Gray lines* indicate the zero-current. *D*, current amplitude comparison of maximal capsaicin-induced currents normalized to maximal menthol-induced currents from *C*, showing the effect of increasing ratios of Gap43-TAD on TRPV1 (n = 5–9 cells). Statistical significance is indicated as *asterisks*, **, $p < 0.005$; ***, $p < 0.001$.

with TRPM8 in *Xenopus* oocytes. Coexpression of TRPV1 and TRPM8 with Gap43-TAD at a 1:1:1 ratio resulted in inhibition of the capsaicin-induced current about 40%. With an increasing ratio of Gap43-TAD (1:1:5, TRPV1:TRPM8:Gap43-TAD), coexpression caused a further inhibition of the capsaicin-induced current (about 75%) as a result of the dominant-negative phenotype of Gap43-TAD (Fig. 6, *C* and *D*). These results further demonstrate that C-terminal residues 69–89 function as TAD to mediate homomeric assembly of functional TRPV1 channels.

Suppression of Dominant-negative Effect of a Poreless TRPV1 Mutant by Deletion of the TAD—To further demonstrate the functional role of the TAD, we generated a TRPV1 deletion mutant (TRPV1 ΔTAD) in which C-terminal residues 69–89 (residues 752–772 of the full-length mTRPV1) were deleted (Fig. 7*A*). As a positive control, co-transfection of WT TRPV1 and TRPM8 (at a 1:1 ratio) into HEK293T cells resulted in an increased calcium signal activated by capsaicin (150 nM) and followed by menthol (500 μM) in the calcium imaging assay (Fig. 7*B*, *top panels*). To further confirm the effect of ΔTAD on channel function, we took advantage of a poreless mutant (plTRPV) in which a partial P-loop (residues 628–646) of TRPV1 was deleted. This poreless mutant ablated the channel function by its dominant-negative effect when co-expressed with WT TRPV1 channels (Fig. 7*B*, *middle panels*), consistent with previous literature for the dominant-negative phenotype of the plTRPV mutant (17). Based on plTRPV1, we constructed a double mutant plTRPV1ΔTAD that carries the deletion of TAD (ΔTAD). We reasoned that removal of the TAD from the poreless mutant (plTRPV1) would diminish the dominant-negative effect of the poreless mutant plTRPV1 on the WT TRPV1 channel by disrupting co-assembly. Cells co-expressing TRPV1 and TRPM8 with the poreless double mutant plTRPV1ΔTAD (1:1:5 ratio, TRPV1:TRPM8:plTRPV1) indeed responded to capsaicin with an increase of intracellular calcium as a result of suppression of its dominant-negative effect from removal of the TAD, which was subsequently confirmed by intact activation of the TRPM8 function by menthol (Fig. 7*B*, *bottom panels*). To further ensure that the poreless double mutant plTRPV1ΔTAD was expressed, we carried out Western blot analysis to detect the protein expression of the mutant. The result shows that the plTRPV1ΔTAD was robustly expressed, further demonstrating that TAD in the C terminus mediates the functional assembly of TRPV channels (Fig. 7*C*).

DISCUSSION

Based on the present findings, we propose that homomeric assembly of the TRPV1 channel is mediated by a tetrameric assembly domain located in the channel C terminus following the TRP-like domain. This conclusion is based on our experimental observations using various approaches of biochemistry, confocal and calcium imaging, as well as electrophysiology. First, we found that the C terminus of TRPV1–4 channels can self-associate to form stable multimers *in vitro* and live cells. Pulldown assay and Western blot analysis have led us to identify a segment within the C terminus necessary for self-association between the C-terminal monomers. Second, we took advantage of the membrane-tethered peptide Gap43 as a tool that is capable of causing a dominant-negative effect at the membrane on wild-type TRPV channels in a concentration-dependent man-

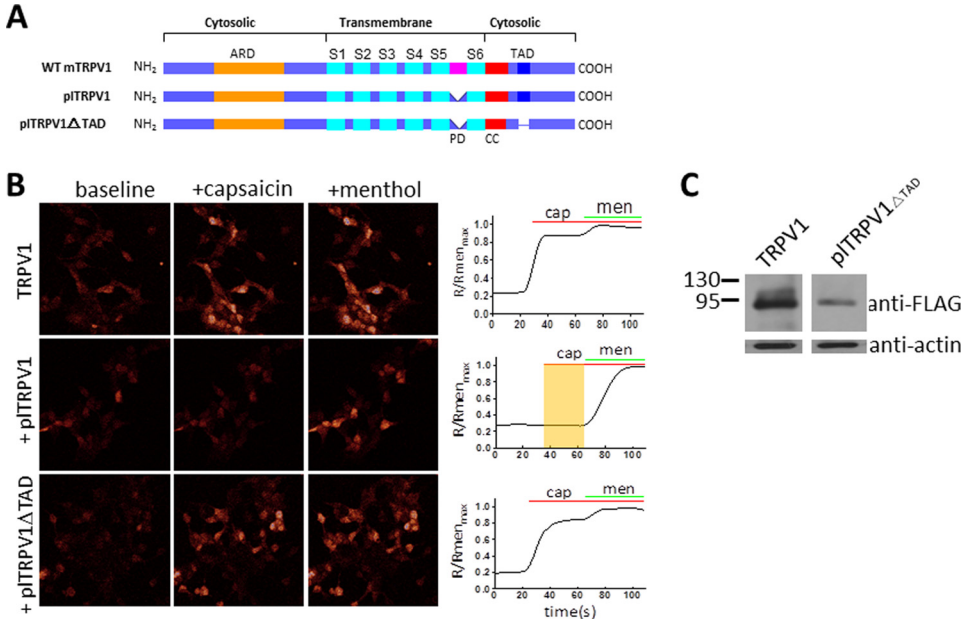

FIGURE 7. **Suppression of negative dominance of the poreless TRPV1 mutant over TRPV1 channel function by deletion of the TAD.** *A,* schematic showing a poreless TRPV1 mutant, and the TAD deletion constructs generated, are based on TRPV1 and the poreless TRPV1 mutant. The *cyan boxes* represent 1–6 transmembrane segments, the *pink box* indicates the pore-loop domain (*PD*, 628–646); *red boxes* in the C terminus illustrate the coiled-coil domain (*CC*); and the *dent* and *thin lines* show deletions of the *p*-loop and 61–80 amino acids at the C terminus, respectively. *B,* calcium imaging of HEK293T cells co-transfected by TRPM8 and TRPV1 or TRPV1 mutants as indicated. *Top panel* indicates co-transfection of TRPV1:TRPM8 at a 1:1 ratio, and the calcium signals were detected in the absence (baseline) or presence of capsaicin and menthol. The *middle panel* indicates co-transfection of TRPV1 and TRPM8 with pITRPV1 at a ratio of 1:1:5 (TRPV1:TRPM8:pITRPV1). The *bottom panel* shows co-transfection of TRPV1 and TRPM8 with pITRPV1△TAD (a double mutation of pITRPV1 and TAD deletion) at a ratio of 1:1:5 (TRPV1:TRPM8:pITRPV1△TAD). *Right panel*, semiquantitative measurements of calcium signals. Normalized traces of calcium signals corresponding to the *left image*, each trace is an average of 24–43 cells. Applications of capsaicin (*cap*, 150 nM) and menthol (*men*, 500 μM) are indicated as *green* and *red lines*, respectively. The *shaded area in yellow* indicates the lack of responses to capsaicin. *C,* Western blotting of the cell lysate of HEK29T transfected with FLAG-tagged TRPV1 and pITRPV1 (*middle panel* in *B*) or TRPV1 and the FLAG-tagged double mutant pITRPV1△TAD (*bottom panel* in *B*), Western blot results are blotted with anti-FLAG or anti-actin, respectively. Molecular mass standards are indicated as kDa.

ner. Our results show that coexpression of the membrane-tethered C terminus prevented WT TRPV channels from forming into homomeric assembly. Furthermore, removal of the TAD in a poreless TRPV1 mutant channel diminishes its dominant-negative effect by disrupting its interaction with WT channels, and rescues the channel function when co-expressed with WT channels. Third, electrophysiological recordings in *Xenopus* oocytes demonstrate that the membrane-tethered TAD can specifically inhibit amplitude of the TRPV1 current by disrupting the channel assembly in a dose-dependent manner. Functional role of the TAD is specific because coexpression of TAD-unrelated proteins had no effect on current amplitude. Together, these data provide compelling evidence that TAD in the C terminus mediates the homotetrameric association of heat-activated TRPV1–4 channels.

We adopted an approach of the Gap43 peptide, which comprises N-terminal 20 amino acids with the membrane-tethering property intact. The membrane-tethered Gap43 (growth-associated protein 43, initially known as F1, B50, and neuromodulin) is a cytoplasmic protein that can be attached to the membrane via a palmitoylation sequence that targets Gap43 to lipid rafts. Gap43 peptide fused with either EGFP or segments of the TRPV channels are expressed well in HEK293T cells, and therefore the Gap43 fusion protein was used as a tool in this study for measurement of its dominant-negative effects on coexpressed proteins. Experiments measuring fluorescence and calcium signal support this idea. Although coexpression of the Gap43 fusion protein and WT TRPV1 channels at a 1:1 ratio in *Xenopus* oocytes only results in about 45% inhibition on channel function (Fig. 4), not 94% inhibition (based on the calculation of binomial distribution for dominant-negative effect on tetramers), this is likely due to either the unequal protein expression or in some degree to Gap43 fusion proteins that can self- or transassociate, compared with WT TRPV1 channels when co-expressed. Observations that increasing the expression ratio of Gap43 fusion proteins leads to more inhibition support the role of TAD in homomeric assembly. The purpose of utilizing Gap43 in this study is to screen and identify domains that are critical for protein-protein interactions, not a quantitative measurement for subunit composition. Therefore, the observed effect of Gap43 with less negative dominance does not alter the conclusion reached here about the TAD identified for critical homomeric assembly of heat-activated TRPV1 channels. In addition, the approach applied here to identify domains mediating homomeric assembly, combined assay of membrane-tethered Gap43, and membrane fluorescence approach may prove applicable for examining the protein-protein interaction of other channel complexes in which cytoplasmic domains are critical for multimerization.

The cytosolic C terminus of TRPV channels contains multiple binding sites and regulatory domains, and has previously been shown to influence channel activity, calcium dependence, and pharmacology in response to capsaicin, proton, and voltage (27, 28). In the C-terminal region, a TRP-like domain, which contains a TRP box following the last transmembrane segment, has been proposed to function as a general conserved association domain that determines subunit multimerization (17). It is

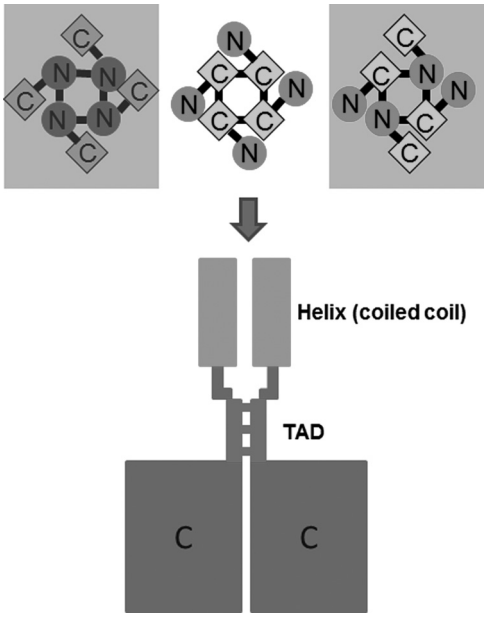

FIGURE 8. **A molecular model for tetrameric assembly of TRPV channels.** *Top panel*, an illustration of three possibilities of homotetrameric assembly mediated by N termini (*left*), C termini (*middle*), and N termini (*right*). Our findings favor that the C terminus mediates the homotetrameric assembly of TRPV1–4 channels (*middle*), not the two framed. *Bottom panel* shows the proposed model of tetramerization mediated by the TAD connecting the coiled-coil domain and the C termini. For clarity, only two of the four subunits are shown.

thought that the TRP-like domain mediated a coiled-coil interaction. However, the role of the proposed coiled-coil domain in tetramerization remains controversial. Disruption of the TRP box domain of TRPV1 by fusion of the corresponding region of either TRPV3 or TRPV4 channels still renders the channel function (31), suggesting that the coiled-coil domain is not essential for tetramerization of TRPV1 and other C-terminal regions may play an important role in channel assembly. This is consistent with our observations that deletion of the coiled-coil domain (first 40 amino acids following the S6 transmembrane domain) still retains the dimeric formation of the channel. A molecular model proposed by Garcia-Sanz *et al.* (17) shows that the TRP-like domain consists of an amphipatic α-helix A, a short α-helix, and a flexible loop that connects to the modulatory domain not involved in subunit-subunit contact. The α-helix A as an association domain forms a four-helix bundle structure, holding the subunits together to produce the homotetramer. The TAD identified in this study coincidently resembles the short α-helix in the proposed model. Together with our findings, we propose that the short α-helical TAD interacts to form another four-helix bundle below the TRP-like domain mediates the homomeric assembly of heat-activated TRPV1 channels (Fig. 8). In conclusion, our results provide evidence that the TAD of heat-activated TRPV1 channels, which resides in the channel C terminus below the TRP-like box, functions to assemble for homotetramers.

Acknowledgments—We thank Xiling Bian, Yiquan Tang, and Xu Cao for discussion and comments on this work. We also thank J. M. Wang for consistent support during this research.

REFERENCES

1. Caterina, M. J., Schumacher, M. A., Tominaga, M., Rosen, T. A., Levine, J. D., and Julius, D. (1997) *Nature* **389,** 816–824
2. Chuang, H. H., Prescott, E. D., Kong, H., Shields, S., Jordt, S. E., Basbaum, A. I., Chao, M. V., and Julius, D. (2001) *Nature* **411,** 957–962
3. Watanabe, H., Vriens, J., Prenen, J., Droogmans, G., Voets, T., and Nilius, B. (2003) *Nature* **424,** 434–438
4. Hille, B. (2001) *Ion Channels of Excitable Membranes,* Third Edition, Sinauer Associates, Inc., Sunderland, MA
5. Clapham, D. E. (2003) *Nature* **426,** 517–524
6. Venkatachalam, K., and Montell, C. (2007) *Annu. Rev. Biochem.* **76,** 387–417
7. Montell, C. (2001) *Sci. STKE* 2001, re1
8. Saito, S., and Shingai, R. (2006) *Physiol. Genomics* **27,** 219–230
9. Montell, C., Birnbaumer, L., and Flockerzi, V. (2002) *Cell* **108,** 595–598
10. den Dekker, E., Hoenderop, J. G., Nilius, B., and Bindels, R. J. (2003) *Cell Calcium* **33,** 497–507
11. Voets, T., Droogmans, G., Wissenbach, U., Janssens, A., Flockerzi, V., and Nilius, B. (2004) *Nature* **430,** 748–754
12. Dhaka, A., Uzzell, V., Dubin, A. E., Mathur, J., Petrus, M., Bandell, M., and Patapoutian, A. (2009) *J. Neurosci.* **29,** 153–158
13. Caterina, M. J. (2007) *Am. J. Physiol. Regul. Integr. Comp. Physiol.* **292,** R64–76
14. Güler, A. D., Lee, H., Iida, T., Shimizu, I., Tominaga, M., and Caterina, M. (2002) *J. Neurosci.* **22,** 6408–6414
15. Hoenderop, J. G., Voets, T., Hoefs, S., Weidema, F., Prenen, J., Nilius, B., and Bindels, R. J. (2003) *EMBO J.* **22,** 776–785
16. Kedei, N., Szabo, T., Lile, J. D., Treanor, J. J., Olah, Z., Iadarola, M. J., and Blumberg, P. M. (2001) *J. Biol. Chem.* **276,** 28613–28619
17. García-Sanz, N., Fernández-Carvajal, A., Morenilla-Palao, C., Planells-Cases, R., Fajardo-Sánchez, E., Fernández-Ballester, G., and Ferrer-Montiel, A. (2004) *J. Neurosci.* **24,** 5307–5314
18. Cheng, W., Yang, F., Takanishi, C. L., and Zheng, J. (2007) *J. Gen. Physiol.* **129,** 191–207
19. Phelps, C. B., Huang, R. J., Lishko, P. V., Wang, R. R., and Gaudet, R. (2008) *Biochemistry* **47,** 2476–2484
20. Gaudet, R. (2008) *Mol. Biosyst.* **4,** 372–379
21. Jin, X., Touhey, J., and Gaudet, R. (2006) *J. Biol. Chem.* **281,** 25006–25010
22. McCleverty, C. J., Koesema, E., Patapoutian, A., Lesley, S. A., and Kreusch, A. (2006) *Protein Sci.* **15,** 2201–2206
23. Lishko, P. V., Procko, E., Jin, X., Phelps, C. B., and Gaudet, R. (2007) *Neuron* **54,** 905–918
24. Numazaki, M., Tominaga, T., Toyooka, H., and Tominaga, M. (2002) *J. Biol. Chem.* **277,** 13375–13378
25. Bhave, G., Hu, H. J., Glauner, K. S., Zhu, W., Wang, H., Brasier, D. J., Oxford, G. S., and Gereau, R. W., 4th (2003) *Proc. Natl. Acad. Sci. U.S.A.* **100,** 12480–12485
26. Prescott, E. D., and Julius, D. (2003) *Science* **300,** 1284–1288
27. Vlachová, V., Teisinger, J., Susánková, K., Lyfenko, A., Ettrich, R., and Vyklický, L. (2003) *J. Neurosci.* **23,** 1340–1350
28. Hellwig, N., Plant, T. D., Janson, W., Schäfer, M., Schultz, G., and Schaefer, M. (2004) *J. Biol. Chem.* **279,** 34553–34561
29. Benowitz, L. I., and Routtenberg, A. (1997) *Trends Neurosci.* **20,** 84–91
30. Wang, H., Yan, Y., Liu, Q., Huang, Y., Shen, Y., Chen, L., Chen, Y., Yang, Q., Hao, Q., Wang, K., and Chai, J. (2007) *Nat. Neurosci.* **10,** 32–39
31. García-Sanz, N., Valente, P., Gomis, A., Fernández-Carvajal, A., Fernández-Ballester, G., Viana, F., Belmonte, C., and Ferrer-Montiel, A. (2007) *J. Neurosci.* **27,** 11641–11650